Molecular Dynamics Simulations of Imidazolium and Pyrrolidinum-Based Ionic Liquids Doped with LiTFSI

Oleg Borodin, Grant D. Smith

Introduction

Room temperature ionic liquids (IL) have been widely investigated for use in lithium batteries,[1, 2] biphasic systems for separation and solvents for synthetic and catalytic applications,[3] actuators[4] and as a reaction media because of negligible vapor pressure, excellent thermal and electrochemical stability, good dissolution properties with many organic and inorganic compounds, and low flammability. Moreover, IL properties can be tailored for a specific chemical (separation, catalysis, reactions) or electrochemical (battery, actuators) application by combining various cations with anions to achieve the desired solvating or transport properties that it turn influence other properties such as Li^+ transport or the rate of chemical reaction or actuator response[4] in a medium.

We present development of an accurate quantum chemistry-based polarizable force field for simulations of (*N*-alkyl-*N*-methylpyrrolidinium)$^+$TFSI$^-$ and methylimidazolium$^+$TFSI$^-$ and their mixtures with LiTFSI. Analysis of MD simulations is focused on understanding the structure of the ILs, mechanisms of the Li^+ transport and the influence of the cation choice (emim$^+$ vs. mppy$^+$) on structural and transport properties of pure ILs and ILs with doped LiTFSI salt. Cooperativity and heterogeneity of ion rotational and translational motion will be examined in light of to recent findings from dielectric[5] and conductivity studies[6] of emim$^+$TFSI$^-$. For example, we will show that the collective relaxation of permanent dipoles in ILs occurs faster than relaxation of individual ions. This is a somewhat unexpected result because the opposite tendency is observed for liquids such as water, ethylene carbonate (EC) or ethers.

The choice of emim$^+$ and mppy$^+$ is dictated by the desire to simultaneously obtain the lowest viscosity and melting point of ILs. Analysis of phase diagrams of a family of (*N*-alkyl-*N*-methylpyrrolidinium)$^+$TFSI$^-$[7] and alkyl-methyl-imidazolium$^+$TFSI$^-$[6] ILs has revealed that their melting points monotonically decrease with increasing length of the alkyl tails. However, longer tails result in undesirable slower ion dynamics and reduce the volume fraction of ionic groups needed to solvate Li^+ salts. [6,7] The mppy$^+$ and emim$^+$ were chosen as a compromise for achieving low melting point (below room temperature) and fast transport. The TFSI$^-$ anion is chosen because of its significant charge delocalization leading to a relatively weak Li$^+$TFSI$^-$ binding[8] and fast conformational dynamics that is expected to promote Li^+ transport. Figure 1(a-b) shows the emim$^+$, mppy$^+$ and TFSI$^-$ ions.

Results and Discussion

A. Force Field Form. Following our previous work[9-13] on lithium transport in carbonate liquid electrolytes, polymer electrolytes and ionic liquids the many-body polarizable form of the force field has been chosen over computationally cheaper and widely used nonpolarizable from. The main reason is this choice is the tendency of two-body nonpolarizable force fields to predict ion transport in IL and Lisalt doped electrolytes up to an order of magnitude slower than experiments[14-17] unless nonbonded parameters are fitted to experimental diffusion data.[18] The potential energy function $U^{tot}(r)$ for the ensemble of atoms, represented by the coordinate vector **r**,

$$U^{tot}(\mathbf{r}) = U^{NB}(\mathbf{r}) + \sum_{bends} U^{BEND}(\theta_{ijk}) + \sum_{tortsions} U^{TORTS}(\phi_{ijkl}) \qquad (1)$$

The contributions due to bends $U^{BEND}(\theta_{ijk})$ and torsions $U^{TORS}(\phi_{ijkl})$ are given by,

$$U^{BEND}(\theta_{ijk}) = \frac{1}{2} k_{\alpha\beta\gamma}^{BEND} (\theta_{ijk} - \theta_{ijk}^{0})^2 \qquad (2)$$

$$U^{TORTS}(\phi_{ijkl}) = \sum_{n} \frac{1}{2} k_{\alpha\beta\gamma\delta}^{TORT} [1 - \cos(n\phi_{ijkl})], \qquad (3)$$

where θ_{ijk} and θ_{ijk}^{0} are the instantaneous and "natural" bending angle for atoms i, j and k, and ϕ_{ijkl} is the dihedral angle for atoms i, j, k and l. The $k_{\alpha\beta\gamma}^{BEND}$ and $k_{\alpha\beta\gamma\delta}^{TORT}$ are the bend force constant and torsional parameter, respectively. The α, β, γ, δ denote atom type for atoms i, j, k and l respectively. Bond lengths were constrained in all simulations to allow use of a larger simulation timestep. The nonbonded energy $U^{NB}(\mathbf{r})$ consists of the sum of the two-body repulsion and dispersion energy $U^{RD}(\mathbf{r})$, the energy due to interactions of fixed charges $U^{coul}(\mathbf{r})$ and the polarization energy $U^{pol}(\mathbf{r})$ arising from the interaction of induced dipoles with fixed charges and other induced dipoles,

$$U^{NB}(\mathbf{r}) = U^{RD}(\mathbf{r}) + U^{coul}(\mathbf{r}) + U^{pol}(\mathbf{r}) =$$

$$\sum_{i>j} \left(A_{\alpha\beta} \exp(-B_{\alpha\beta} r_{ij}) - C_{\alpha\beta} r_{ij}^{6} + D\left(\frac{12}{B_{\alpha\beta} r_{ij}}\right)^{12} \right) + \sum_{i>j} \left(\frac{q_i q_j}{4\pi\varepsilon_0 r_{ij}} \right) - 0.5 \sum_{i} \vec{\mu}_i \vec{E}_i^{0}, \qquad (4)$$

Here the induced dipole at a force center i is $\vec{\mu}_i = \alpha_i \vec{E}_i^{tot}$, α_i is the isotropic atomic polarizability, $\vec{E}_i^{tot}$ is the total electrostatic field at the atomic site i due to permanent charges q_j and induced dipoles $\vec{\mu}_j$, ε_0 is the dielectric permittivity of vacuum, $\vec{E}_i^{0}$ is the electric field due to fixed charges only, $A_{\alpha\beta}$ and $B_{\alpha\beta}$ are the repulsion parameters and $C_{\alpha\beta}$ is the dispersion parameter for interaction between atoms i and j that have atom types α,β. The term $D\left(\frac{12}{B_{\alpha\beta} r_{ij}}\right)^{12}$, D= 0.0005 kcal/mol is essentially zero at typical atom approaches, but becomes the dominant term at $r_{ij} < 1$ Å ensuring that $U^{RD}(\mathbf{r})$ is repulsive at unphysical close atom approaches. We also used the Thole screening that smears induced dipoles in order to prevent polarization catastrophe from occurring as previously described.[9] The interaction between an induced dipole and a partial charge separated by 3 bonds was scaled by 0.8.

The force field parameters for the TFSI/TFSI⁻ and Li⁺/TFSI⁻ interactions, the repulsion-dispersion parameters for the emim⁺ and mppy⁺ cation interactions with TFSI⁻ and Li⁺ were taken directly from the previously developed quantum chemistry-based force field for oligoethers, alkanes, carbonates doped with LiTFSI.[10] Bonds, bends and torsions and partial charges were fitted for quantum chemistry data. For a detailed description of the simulation methodology employed in the study of the LiTFSI doped ILs the reader is referred our previous papers detailing simulations of pure ILs.[19, 20]

MD simulations predicted densities of ILs in good agreement with experiments as shown in Table 1.

Table 1. Properties of ILs from MD simulations.

Temp. (K)	NPT run (ns)	NVT run (ns)	Density, MD (kg/m^3)	Density exp. (kg/m^3)	ΔH^{vap} (kJ/mol)	ΔH^{vap} (J/cm^3)	$\Delta U^{cat/anion}$ (kJ/mol)
				emimTFSI			
393	1	11.5	1404	1427[a]	96	335	-350
363	0.5	8	1431	1457[a]	99	351	-352
333	1	10	1463	1487[a], 1484[b]	102	370	-353
303	1	9	1497	1517[a],1514[b], 1516.6[c]	105	393	-355
				mppyTFSI			
500	0.5	1.1	1216				
393	1.0	16.2	1312		108	336	-339
333	0.8	8	1369	1386[d]	114	373	-342
303	1	13.2	1401	1405[d]	117	394	-344

b from ref. [21]
c interpolation from [22]
d from ref. [23]

Energy density of emim$^+$TFSI$^-$ and mppy$^+$TFSI$^-$ ILs was characterized by calculating enthalpy of vaporization ΔH^{vap} from the liquid into gas phase containing cation/anion dimers and the average cation/anion binding energy U$^{cat/anion}$ in the gas phase as shown in Table 2. The enthalpy of vaporization per mol of emim$^+$TFSI$^-$ was ~10% or 12kJ/mol lower than that for mppy$^+$TFSI$^-$, while the magnitude of the average cation/anion binding energy is 12 kJ/mol or 3-4% higher for emim$^+$TFSI$^-$ compared to mppy$^+$TFSI$^-$. The later one agrees well with the energy difference of 10 kJ/mol for the most stable emim$^+$/TFSI$^-$ and mppy$^+$/TFSI$^-$ dimers of 330 kJ/mol and 340 kJ/mol obtained from quantum chemistry calculations[19, 24] at the MP2/6-31G** and MP2/6-31G* levels, respectively. Smaller magnitude of the cation/anion binding energy from quantum chemistry calculations is attributed to reduced dispersion interactions in quantum chemistry calculations due to incomplete basis set as previously discussed.[19] Note, that the total cohesive energy density of both ILs vs. isolated ion state is very similar.
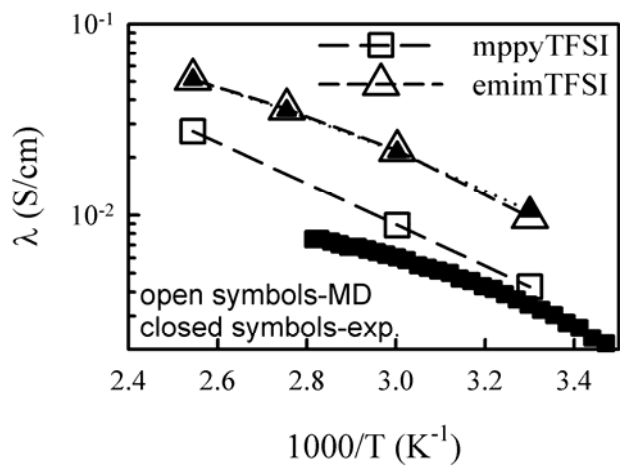
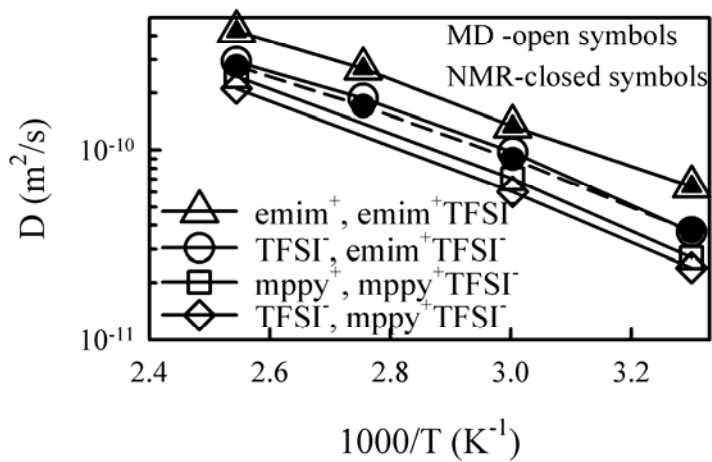Figure 1. Conductivity of ILs from experiments and MD simulations.

Figure 2. Ion self-diffusion coefficients from experiments and MD simulations.
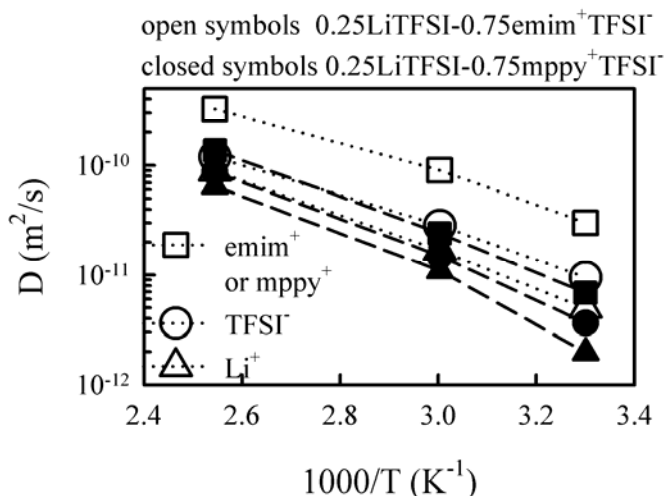
Figure 3. Comparison of ion conductivity from MD simulations for emim[+]TFSI[-] and mppy[+]TFSI[-] ILs doped with LiTFSI.

The predicted and experimental[6, 23] ion self-diffusion coefficients and conductivities for pure ILs and ILs doped with 0.25 mol of LiTFSI are shown in Figures 1-3. Good agreement between predicted and experimental data is observed. The quality of the agreement between experimental data and MD simulations results is especially encouraging because nonbonded parameters were not fit to any data for ILs, and, thus, show good transferability from our previously developed quantum chemistry-based force fields for polymeric and liquid electrolytes.

Li^{+} Transport Mechanism
MD simulations give us the unique ability to estimate the structure diffusion contribution to the Li^{+} diffusion coefficient by performing simulations in which we add an additional function (see eq. 1) in order to dramatically slow down the exchange of TFSI[-] anions in the Li^{+} first coordination shell during the simulations, while preserving the structure of the first Li^{+} coordination shell. Indeed, the additional Li^{+}-O[TFSI-] function does not shift the first peak of the Li^{+}-O[TFSI-] position in the MD simulations, but does increase its magnitude from 26 to 90. The number of O[TFSI-] in the Li^{+} first coordination shell is 4, which is essentially the same as in simulations without this additional function. However, increasing the Li^{+}-O[TFSI-] interactions results in an increase of the Li^{+}-O[TFSI-] residence times by a factor of 12 and 5 for the 0.25LiTFSI-0.75mppy[+]TFSI[-] and 0.25LiTFSI-0.75mmpy[+]TFSI[-] ILs, respectively. With the modified potential the TFSI[-] molecules in the Li^{+} first coordination shell are essentially moving together with the Li^{+} cations on the scale of multiple solvent diameters. Preliminary analysis indicates that a similar Li^{+} cation transport mechanism is present in the emim[+]TFSI[-] IL doped with LiTFSI.

Mechanical Properties

her the shear modulus of an electrolyte the higher its dendrite suppression ability of the membrane. We calculated the short time shear moduli of ILs and compared them with those for PEO/LiTFSI and EC in order to check for correlations between short time/high frequency mechanical properties and ability of electrolyte to suppress dendrite at a certain current.

The shear transverse stress relaxation modulus G(t) can be calculated from MD simulations using time autocorrelation function of the stress tensor

$$G(t) = \frac{V}{k_B T} \left\langle P_{\alpha\beta}(t) P_{\alpha\beta}(0) \right\rangle \qquad (5)$$

where $P_{\alpha\beta}(t)$ is an instantaneous value of the off-diagonal element of the stress tensor at time t, V is the volume of the system and the brackets denote the averaging over the whole trajectory. The fits to the time dependent shear modulus G(t) obtained from simulations are shown in Figure 14 for LiTFSI doped ILs, PEO/LiTFSI and EC. Addition of LiTFSI to mppy$^+$TFSI$^-$ increases both relaxation time for G(t) and glassy modulus given by short time (high frequency) value of shear modulus as shown in Figure 4a. Comparison of G(t) for ILs, PEO/LiTFSI and EC is shown in Figure 4b. Intriguingly, the sub-nanosecond shear modulus of ILs and PEO/LiTFSI are very similar. The time dependent shear modulus for EC is significantly smaller in magnitude and decays much faster than that for ILs and polymer. Thus, we summarize that mechanical behavior of the simulated ILs is much closer to that of polymer electrolytes such as PEO/LiTFSI than regular polar liquid-based electrolytes such as EC/LiTFSI at timescales shorter than Rouse time.
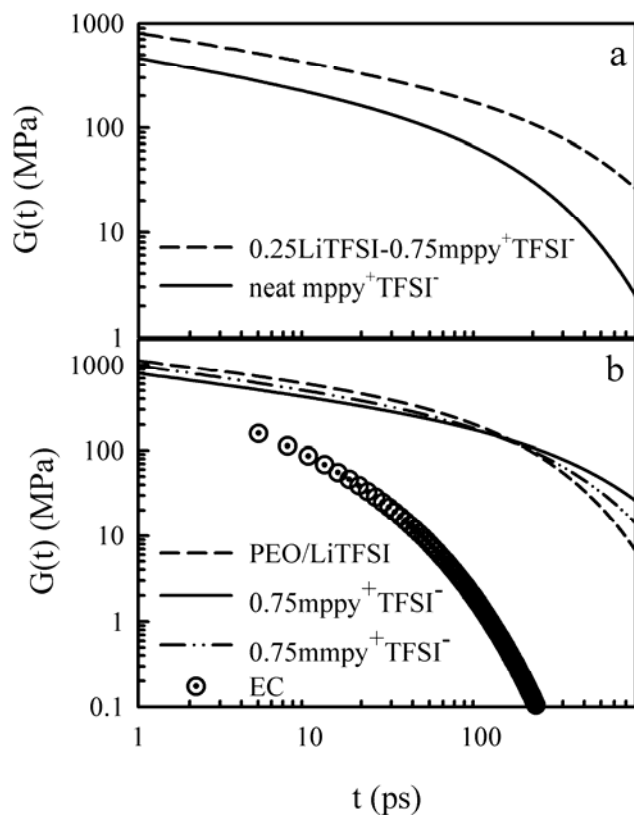

Figure 4. The stretched exponential fits to the time-dependent shear modulus data for ILs doped with

LiTFSI at 333 K, PEO(Mw=2380)/LiTFSI,[12] EO:Li=20 at 333 K and EC/LiTFSI,[11] EC:Li=10 at 313

K.

References

1.	Seki, S.; Kobayashi, Y.; Miyashiro, H.; Ohno, Y.; Usami, A.; Mita, Y.; Watanabe, M.; Terada, N. *Chemical Communications* **2006**, 544-545.
2.	Shin, J. H.; Henderson, W. A.; Passerini, S. *Electrochemistry Communications* **2003,** *5*, 1016-1020.
3.	Forsyth, S. A.; Pringle, J. M.; MacFarlane, D. R. *Australian Journal of Chemistry* **2004,** *57*, 113-119.
4.	Ding, J.; Zhou, D.; Spinks, G.; Wallace, G.; Forsyth, S.; Forsyth, M.; MacFarlane, D., Use of Ionic Liquids as Electrolytes in Electromechanical Actuator Systems Based on Inherently Conducting Polymers. In *Chem. Mater.*, 2003; Vol. 15, pp 2392-2398.
5.	Daguenet, C.; Dyson, P. J.; Krossing, I.; Oleinikova, A.; Slattery, J.; Wakai, C.; Weingartner, H., Dielectric Response of Imidazolium-Based Room-Temperature Ionic Liquids. In *J. Phys. Chem. B*, 2006; Vol. 110, pp 12682-12688.
6.	Tokuda, H.; Hayamizu, K.; Ishii, K.; Susan, M. A. B. H.; Watanabe, M. *Journal of Physical Chemistry B* **2005,** *109*, 6103-6110.
7.	Henderson, W. A.; Passerini, S. *Chemistry of Materials* **2004,** *16*, 2881-2885.
8.	Tarascon, J. M.; Armand, M. *Nature* **2001,** *414*, 359-367.
9.	Borodin, O.; Smith, G. D. *J. Phys. Chem. B* **2006,** *110*, 6279-6292.
10.	Borodin, O.; Smith, G. D. *J. Phys. Chem. B* **2006,** *110*, 6293-6299.
11.	Borodin, O.; Smith, G. D. *J. Phys. Chem. B* **2006,** *110*, 4971-4977.
12.	Borodin, O.; Smith, G. D. *Macromolecules* **2006,** *39*, 1620-1629.
13.	Borodin, O.; Smith, G. D.; Douglas, R. *Journal of Physical Chemistry B* **2003,** *107*, 6824-6837.
14.	Bhargava, B. L.; Balasubramanian, S. *Journal of Chemical Physics* **2005,** *123*, 144505.
15.	Rey-Castro, C.; Vega, L. F. *Journal of Physical Chemistry B* **2006,** *110*, 14426-14435.
16.	Cadena, C.; Zhao, Q.; Snurr, R. Q.; Maginn, E. J. *J. Phys. Chem. B* **2006,** *110*, 2821-2832.
17.	Borodin, O.; Smith, G. D.; Jaffe, R. L. *Journal of Computational Chemistry* **2001,** *22*, 641-654.
18.	Micaelo, N. M.; Baptista, A. M.; Soares, C. M. *J. Phys. Chem. B* **2006,** *110*, 14444-14451.
19.	Borodin, O.; Smith, G. D. *J. Phys. Chem. B* **2006,** *110*, 11481-11490.
20.	Borodin, O.; Smith, G. D.; Henderson, W. *J. Phys. Chem. B* **2006,** *110*, 16879 -16886.
21.	Krummen, M.; Wasserscheid, P.; Gmehling, J. *Journal of Chemical and Engineering Data* **2002,** *47*, 1411-1417.
22.	Fredlake, C. P.; Crosthwaite, J. M.; Hert, D. G.; Aki, S. N. V. K.; Brennecke, J. F. *Journal of Chemical and Engineering Data* **2004,** *49*, 954-964.
23.	Nicotera, I.; Oliviero, C.; Henderson, W. A.; Appetecchi, G. B.; Passerini, S. *Journal of Physical Chemistry B* **2005,** *109*, 22814-22819.
24.	Tsuzuki, S.; Tokuda, H.; Hayamizu, K.; Watanabe, M. *Journal of Physical Chemistry B* **2005,** *109*, 16474-16481.